Strain relaxation in $Fe_3O_4/MgAl_2O_4$ heterostructures: Mechanism for formation of antiphase boundaries in an epitaxial system with identical symmetries of film and substrate

M. Luysberg,[1] R. G. S. Sofin,[2,*] S. K. Arora,[2] and I. V. Shvets[2]
[1]*Institut für Festkörperforschung und Ernst Ruska-Centrum, Forschungszentrum Jülich, D-52425 Jülich, Germany*
[2]*Centre for Research on Adaptive Nanostructures and Nanodevices (CRANN), School of Physics, Trinity College Dublin, Dublin 2, Ireland*

(Received 23 April 2009; published 15 July 2009)

Strain relaxation studies in epitaxial magnetite, Fe_3O_4, thin films grown on $MgAl_2O_4(100)$ substrates are reported. The study shows that the films were relaxed in line with the theoretical model prediction with a critical thickness, $t_c=5$ nm. Antiphase boundaries (APBs) are not expected to form in Fe_3O_4 films grown on $MgAl_2O_4$ substrates because both film and substrate have the same crystal symmetry. In contrast, our study reveals the formation of APBs within the Fe_3O_4 films. Our analysis shows that the APBs in a $Fe_3O_4/MgAl_2O_4$ heteroepitaxial system are formed by partial dislocations, which accommodate the misfit. This formation mechanism of APBs is fundamentally different from the one found in the Fe_3O_4/MgO system, where APBs are formed as a consequence of equivalent nucleation sites on the MgO substrate separated by nontranslational vectors of the Fe_3O_4 lattice. The mechanism for the formation of antiphase boundaries through partial dislocations should be applicable to a wide range of epitaxial systems having identical symmetries of the film and the substrate and significant lattice mismatch.

DOI: 10.1103/PhysRevB.80.024111 PACS number(s): 81.15.Hi, 68.55.−a, 75.50.Bb

I. INTRODUCTION

Magnetite (Fe_3O_4) is one of the potential half-metallic ferrimagnetic materials for the realization of future spin electronic devices due to its high spin polarization, high Curie temperature (858 K), and the metal-to-insulator transition occurring at ~120 K, called the Verwey transition.[1–6] Once developed, applications of this material in devices such as spin valves or magnetic tunnel junctions will likely be in the form of thin films[7–10] and for that, one needs a better understanding of the strain status of the films and how to control the stoichiometry and defect density. The stoichiometry, strain, and defect structure play an important role in determining the magnetotransport and magnetic properties of Fe_3O_4 films.[7,11–16]

Fe_3O_4 has an inverse spinel structure with a lattice constant of 0.83987 nm. There are many reports on the growth of Fe_3O_4 thin films on different types of substrates such as MgO, $MgAl_2O_4$, sapphire, Si, or GaAs, using a variety of deposition techniques.[11,17–25] MgO, which has a rocksalt crystal structure, is a widely used substrate for epitaxy of magnetite due to the small lattice mismatch of 0.33%.[20,21] Antiphase boundaries (APBs) are observed in Fe_3O_4 epitaxially grown onto MgO(100) substrates.[11,17–21] Since the Fe_3O_4 ($Fd\bar{3}m$) crystal structure is lower in symmetry than that of MgO ($Fm3m$), there are several equivalent nucleation sites on the MgO(100) surface, which enforce the formation of APBs at the junction of neighboring grains. The APBs, which can be envisaged as the disruption of cation chains in a continuous oxygen lattice, lead to new magnetic exchange interactions, which are not present in the bulk material.[21] The exchange interactions occurring across the APBs are predominantly antiferromagnetic and the spin-polarized electrons find additional scattering potentials across these antiferromagnetically coupled APBs, which explains the observation of negative magnetoresistance in Fe_3O_4 thin films grown on MgO substrates.[26,27] In a recent report, Kasama *et al.* argued that the oppositely polarized conduction electrons from neighboring domains are antiferromagnetically coupled across the APB explaining the low spin polarization observed in magnetite films grown on MgO(100) substrates.[15] In our recent report we demonstrated that the APBs relate to the observation of the absence of strain relaxation. Even at a film thickness that is ten times greater than the theoretically predicted critical thickness value in the Fe_3O_4/MgO heteroepitaxy system there was little strain relaxation observed.[28] There are many recent reports on the effect of APBs on the magnetic behavior[10,12,14,16,29] and the electrical transport properties[11,13] of Fe_3O_4 thin films grown on a variety of substrates.

$MgAl_2O_4$ is another important substrate used for Fe_3O_4 heteroepitaxy, which finds applications in the fabrication of multilayer devices.[8] $MgAl_2O_4$ has the normal spinel structure and the lattice constant is 0.80831 nm,[30] in which Mg^{2+} and Al^{3+} ions occupy the tetrahedral and octahedral sites, respectively. For $Fe_3O_4/MgAl_2O_4$ the lattice mismatch of 3.4% is about ten times larger than that for the Fe_3O_4/MgO system. Therefore, plastic relaxation is to be expected to occur already at a small film thickness. Since $MgAl_2O_4$ has the same spinel-type crystal structure and symmetry as Fe_3O_4, the formation of APBs is not expected for films grown on $MgAl_2O_4$.[30,31] However, the presence of APBs in the $Fe_3O_4/MgAl_2O_4$ system has been reported.[30,32] Kale *et al.*[23] explained some of the anomalous features observed in the magnetic properties of Fe_3O_4 films on MgO and $MgAl_2O_4$ substrates on the basis of critical-thickness calculations. Although there are many reports on the magnetic, electrical transport, and structural properties of the $Fe_3O_4/MgAl_2O_4$ heteroepitaxy system, a detailed study on strain relaxation and a clear understanding on the formation of APBs in this system is lacking.[23,24] This system is a representative example of an epitaxial system in which the film and the sub-

strate have an identical symmetry but a large lattice mismatch. In contrast to our observations, one would not expect to observe the formation of APBs. Therefore the significance of the study goes well beyond the specific system $Fe_3O_4/MgAl_2O_4$. It could be applicable to systems such as GaAs/Si or $CoFe_2O_4/Fe_3O_4$.[33,34]

In this paper the strain-relaxation behavior of Fe_3O_4 film grown by molecular-beam epitaxy (MBE) onto $MgAl_2O_4$ is investigated. We find the formation of misfit dislocations with partial Burgers vectors responsible for the nucleation of APBs.

II. EXPERIMENTAL

The Fe_3O_4 films of varying thickness in the range of 5–120 nm were deposited under identical growth conditions on (100)-oriented $MgAl_2O_4$ single-crystal substrates (cut along the ⟨100⟩ direction within $\pm 0.2°$) using an oxygen plasma assisted MBE system (DCA MBE M600) with a base pressure of 2×10^{-10} Torr. The substrates were cleaned *in situ* at 600 °C in a 5×10^{-6} Torr oxygen atmosphere for 2 h. Growth of the Fe_3O_4 films was carried out at a substrate temperature of 250 °C from a pure metallic Fe source by means of electron-beam evaporation and oxygen-free radicals generated by an electron cyclotron resonance plasma source. The plasma source was operated at a power of 80 W in an oxygen partial pressure of 1×10^{-5} Torr. Reflection high-energy electron diffraction (STAIB Instruments) was used to monitor the growth mode and growth rate of 0.3 Å/s.

Magnetization measurements were performed using an alternating-gradient field magnetometer (Micromag-3900, Princeton Measurements, USA) with a sensitivity of 10^{-8} emu. The magnetization versus field (*M-H*) loops were measured at room temperature by applying the magnetic field (maximum field of 1 T) in the film plane along the ⟨100⟩ direction. The diamagnetic contribution from the $MgAl_2O_4$ substrate was subtracted from the measured data by performing *M-H* loops of the $MgAl_2O_4$ substrate of similar dimensions as that of the thin-film sample, in the same field range. The uncertainty in measuring the absolute value of magnetization for the films was about 1%.

For structural characterization of Fe_3O_4 thin films, high-resolution x-ray diffraction (HRXRD) measurements were performed using a multicrystal high-resolution x-ray diffractometer (Bede-D1, Bede, UK). The high-resolution x-ray diffractometer in double or triple axis configuration was performed to confirm the epitaxial relationship of the $Fe_3O_4/MgAl_2O_4$ heteroepitaxy. The in-plane ($a_\parallel$) and out-of-plane ($a_\perp$) lattice parameters were determined from the analysis of ω-2θ scans performed around the symmetric (400) and asymmetric (622) diffraction planes common to substrate and film. When operated in triple axis configuration, this instrument can detect lattice-constant variations ($\Delta a/a$) as low as 2×10^{-6} and enables precise determination of the strain relaxation.[28]

Transmission electron microscopy (TEM) was employed to study the coherency of the interface between the Fe_3O_4 and $MgAl_2O_4$ substrate and the morphology of the APBs, using cross-sectional and plan view samples. Mechanical thinning and Ar ion milling was applied to obtain electron transparent areas within the TEM specimen. Structural defects were identified by conventional TEM using a Philips CM 20 electron microscope operated at 200 kV. High-resolution images were obtained with a Philips CM 200 electron microscope, which was equipped with a CEOS double hexapole corrector. Adjusting a negative spherical aberration constant, C_s, of -40 μm and using the optimum over focus setting of the objective lens of 12 nm resulted in a directly interpretable bright-atom contrast and in minimized delocalizations.[35]

III. RESULTS

Magnetization measurements show that Fe_3O_4 films grown on $MgAl_2O_4$ substrates show lower saturation magnetization (M_s) as compared to the saturation magnetization of bulk Fe_3O_4 (480 emu/cm^3). The observed M_s for 15, 60, and 120 nm films are 473, 460, and 466 emu/cm^3, respectively. Thicker films show a lower M_s compared to the thinner 15 nm film. The observation of a reduced M_s and the inability to saturate epitaxial Fe_3O_4 films have been attributed to the presence of APBs.[20,21] Resistivity values for these films measured at 300 K were found to decrease with an increase in thickness. The resistivity values observed at 300 K for these films are 0.0099 and 0.0088 Ω cm for 70- and 120-nm-thick films, respectively. The Verwey transition temperatures for these films were found to be 122 and 123 K for 70- and 120-nm-thick films, respectively, and are higher than those for Fe_3O_4 films deposited on MgO substrates.[28] The value of the Verwey transition temperature is close to the value observed for bulk Fe_3O_4 (~123 K). As the Verwey temperature is highly sensitive to deviations from stoichiometry, its presence in all the films confirms that the films consist of stoichiometric magnetite.[36,37]

To know precisely the extent of strain relaxation for a thickness above 15 nm we employed the HRXRD technique. Figure 1(a) shows the ω-2θ scans of 15-, 60-, and 120-nm-thick Fe_3O_4 films grown on a $MgAl_2O_4$ oxide substrate measured for (400) Bragg planes. The curves are shifted on the vertical axis for clarity. The full width at half maximum of the thin-film peaks are 0.301°, 0.080°, and 0.076°, respectively. The substrate-film peak separation decreases with an increase in thickness. The $a_\perp$ values determined from the film-substrate peak separation are 0.8457, 0.8441, and 0.8408 nm for 15-, 60-, and 120-nm-thick films, respectively.

Figure 1(b) shows ω-$n\theta$ scans measured for the asymmetric (622) Bragg planes in grazing exit geometry for the 60- and 120-nm-thick films. The experimentally measured angular ratio n of the angle included by the x ray to the detector ($n\theta$) and sample (ω) was 2.4 and 2.2 for the 60 and 120 nm films, respectively. A value n other than 2 was required to detect the thin-film peak through a single ω-$n\theta$ scan due to the strain-induced tilt. The $a_\parallel$ determined from the (622) scan is 0.834 and 0.8371 nm for the 60 and 120 nm films, respectively. This corresponds to a relaxation of 70% and 95%. The in-plane and out-of-plane lattice parameters determined from the asymmetric (622) scans agree well with the estimates of

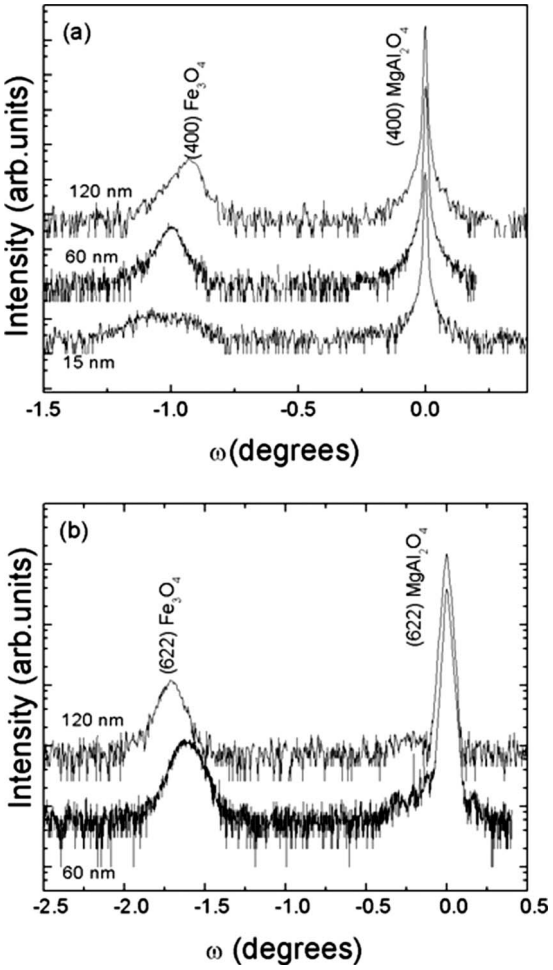

FIG. 1. (a) The ω-2θ scans performed on 15, 60, and 120 nm Fe_3O_4 films grown on (100) $MgAl_2O_4$ substrate measured for symmetric (400) Bragg reflection. Curves are shifted on the vertical axis for clarity. (b) The ω-$n\theta$ scans performed on 60 and 120 nm Fe_3O_4 films grown on (100) $MgAl_2O_4$ substrate measured for asymmetric (622) Bragg reflection (measured in the grazing exit geometry).

strain relaxation for the n ratio used to perform the asymmetric scans. The strain relaxation was measured as a function of thickness in Fe_3O_4 thin films grown on $MgAl_2O_4$ and it was found that the amount of strain relaxation increases with an increase in thickness.

The dark field TEM images shown in Fig. 2 reveal antiphase boundaries for both a 70- and a 200-nm-thick Fe_3O_4 film grown onto $MgAl_2O_4$. Due to the imaging conditions chosen, APBs with shift vector $\frac{a}{4}[110]$ show bright contrasts. Clearly, the density of APBs is observed to decrease with increasing film thickness.

Figure 3 displays the 70-nm-thick Fe_3O_4 film in cross section. Two different two-beam imaging conditions were employed. Choosing a (040) imaging vector [Fig. 3(a)] produces an alternating black and white contrast at the interface, which is caused by misfit dislocations seen end on. Under (004) two-beam imaging conditions [Fig. 3(b)] the contrast of the misfit dislocation vanishes, i.e., the Burgers vector of the dislocations lies within the (004) plane. From these observations the dislocations can be concluded to be sessile

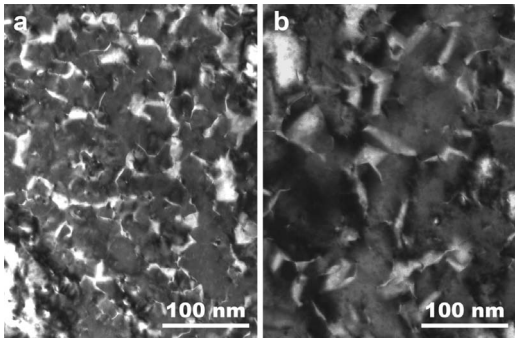

FIG. 2. TEM dark field images in plan view of (a) 70 and (b) 200 nm Fe_3O_4 films on $MgAl_2O_4$ substrate. According to the (220) imaging conditions chosen, APBs with shift vector $\frac{1}{4}[110]$ appear bright.

since the line direction and the Burgers vector are located within the (004) plane, which is not to be known as glide plane for the spinel crystal structure. Contrast fluctuations within the Fe_3O_4 film arise from APBs and/or local strain variations.

The interface between Fe_3O_4 and $MgAl_2O_4$ is viewed at higher magnification in the high-resolution TEM image shown in Fig. 4. Due to the adjustment of a negative spherical aberration constant and the defocus of 12 nm in the aberration-corrected Philips CM 200 microscope, white atom contrast is established.[35] This allows in some areas of the image the assignment of the individual atom columns, e.g., as Fe-O columns and Fe columns within the Fe_3O_4 (see insets of the schematics displaying one unit cell). Due to local strain variations the contrast pattern within the image is ob-

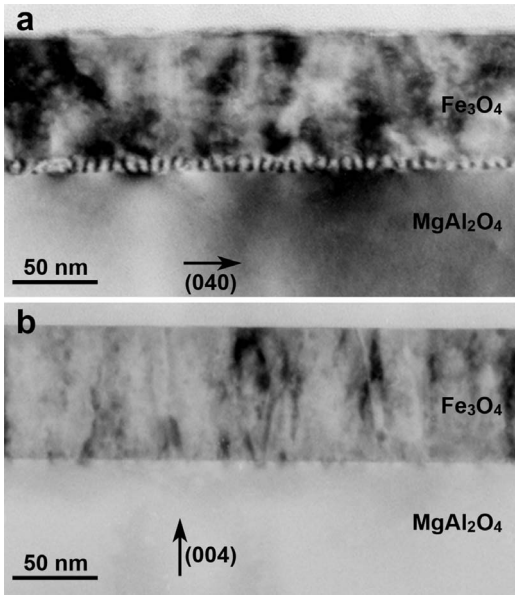

FIG. 3. Cross-sectional TEM bright field images of 70-nm-thick Fe_3O_4 film on $MgAl_2O_4$ substrate. Misfit dislocations are seen at the interface, when a two-beam imaging conditions with a (040) imaging vector is established (a). Under (004) imaging conditions (b) the dislocation contrast vanishes. Contrast fluctuations within the Fe_3O_4 layer are caused by strain and/or APBs.

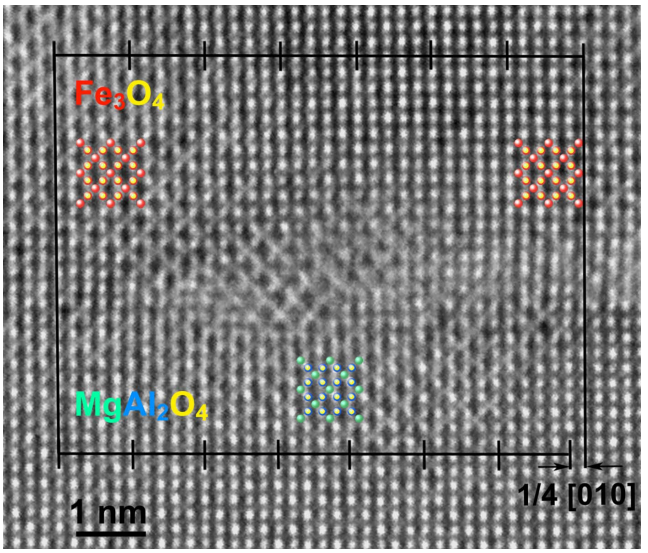

FIG. 4. (Color online) High-resolution TEM image of the interfacial region between Fe_3O_4 and $MgAl_2O_4$. The Burgers circuit indicates a closing vector of $\frac{1}{4}[010]$. This Burgers vector component seen in the (100) projection does not comply with a translation vector of the lattice, i.e., a partial dislocation is formed. Accordingly, an antiphase boundary is formed between the left and right parts of the figure. Due to local strain fields neither the atomic structure of the dislocation core nor that of the APB are resolved. Unit cells of Fe_3O_4 and $MgAl_2O_4$ are schematically displayed as insets (Fe: red, O: yellow, Mg: green, Al: blue).

served to vary. In particular, close to the core of a dislocation the contrast becomes blurred and therefore prevents a closer inspection of the atomic structure.

However, a misfit dislocation is unambiguously identified by the Burgers circuit, which reveals a closing vector of $\frac{1}{4}[010]$. Since the projection of a three-dimensional structure to a two-dimensional one is inherent to the TEM experiment, only the Burgers vector component perpendicular to the viewing direction is detectable. This implies that the "true" Burgers vector can have an additional component in the viewing direction, i.e., along the [100] direction. Dislocations with Burgers vectors $\frac{1}{4}[110]$ and $\frac{1}{4}[010]$ result in the same closing vector of the Burgers circuit in (100) projection. Although we cannot determine the exact Burgers vector, we can nonetheless conclude that the misfit dislocation seen in Fig. 4 is a partial dislocation, i.e., the Burgers vector is not a translational vector of the lattice. In consequence, an APB is associated with the misfit dislocation, which separates the left and right parts of the Fe_3O_4 film by a shift of $\frac{1}{4}[010]$ in the (100) projection.

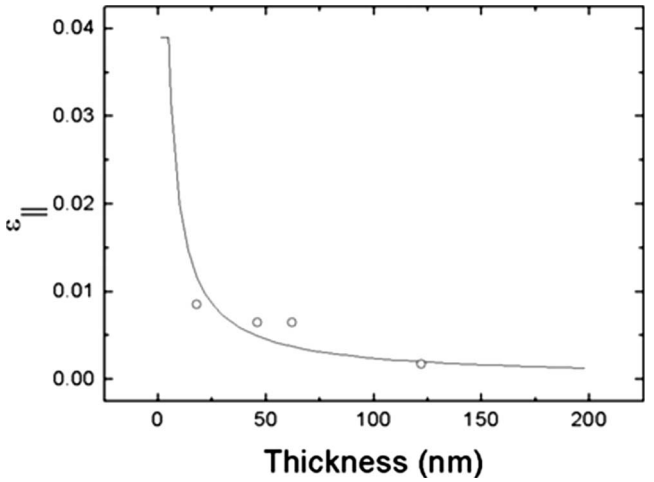

FIG. 5. Comparison of experimentally observed values of the in-plane strain, $\varepsilon_{\parallel}$, with the FKR model predictions for the Fe_3O_4 films grown on $MgAl_2O_4$ (100) substrates as a function of thickness. The solid line is the theoretical prediction and scattered points are experimentally observed values.

IV. DISCUSSION

The Fe_3O_4 films grown onto $MgAl_2O_4$ show an increasing relaxation with increasing film thickness (see Fig. 1 and Table I). In the following we employ the Fischer, Kuhne, and Richards (FKR) model[38] to estimate the critical thickness of a heteroepitaxial system above which the system exhibits strain relaxation. The critical thickness given by this model is

$$t_c = \frac{b\cos\lambda}{\varepsilon_{\parallel}}\left\{1 + \ln\left(\frac{t_c}{b}\right)\left[\frac{1-\frac{\nu}{4}}{4\pi(1+\nu)\cos^2\lambda}\right]\right\}, \qquad (1)$$

where b is the Burgers vector, $\varepsilon_{\parallel}$ is the misfit strain $[\varepsilon_{\parallel} = (a_f - a_s)/a_s]$, ($a_f$ and a_s being the film and substrate lattice parameters), ν is the Poisson ratio, and λ is the angle between the Burgers vector and the direction in the interface normal to the dislocation line. By using the experimentally obtained value of $\nu = 0.30$ (estimated by measuring $a_{\parallel}$ and $a_{\perp}$ from the asymmetric Bragg reflection scans performed in grazing exit and grazing incidence modes), this model gives a value for t_c of 5 nm for the $Fe_3O_4/MgAl_2O_4$ system. Here a Burgers vector value of 0.57442 nm for $MgAl_2O_4$ was assumed, which complies with the shortest translational vector of the lattice, i.e., $a_s/\sqrt{2}$ [110].

Figure 5 shows the calculated equilibrium in-plane strain,

TABLE I. Summary of the predicted and observed strain relaxation values for the epitaxial magnetite films as a function of film thickness.

Sample	Thickness	Strain relaxation predicted by FKR model (%)	Observed strain relaxation (%)
$Fe_3O_4/MgAl_2O_4$	40	87	60
	60	91	84
	120	95	95.6

$\varepsilon_{\|}$, using the FKR model for Fe_3O_4 films on the $MgAl_2O_4$ substrate as a function of thickness along with the measured experimental data. The observed relaxation behavior is in agreement with the values estimated from the model for Fe_3O_4 films grown on $MgAl_2O_4$. Calculated and observed strain relaxation values are given in Table I. In agreement with the strain measurement, misfit dislocations are detected, which cause the relaxation of the Fe_3O_4 films.

In general, the formation of APBs is not to be expected for heteroepitaxial systems of the same crystallographic structure such as $MgAl_2O_4$ and Fe_3O_4. However, our observations clearly demonstrate that APBs are the prominent crystallographic defects within the epitaxial Fe_3O_4 films. This is in agreement with previous reports,[30,32] although there are no mechanisms proposed earlier for the formation of APBs in this system. As the films grow thicker the density of APBs is decreased. This can be attributed to the annihilation of APBs. Since the APBs are inclined with respect to the growth direction (see Figs. 2 and 3), APBs will eventually meet as the films grow thicker. If APBs of the same shift vector join, they annihilate at the apex. From the magnetization data it could be interpreted that the density of APBs in 60 nm film is greater than that of 15 nm film since the former shows lower magnetization compared to the latter. The situation could be a bit more complex. Below t_c there could be no APBs and they are formed once the misfit dislocations are formed at t_c. Then gradually with increasing thickness they annihilate.

The formation of the APBs can be attributed to the generation of misfit dislocations. The misfit dislocation seen in Fig. 4 comprises a partial Burgers vector. This implies that a shift of the lattice is introduced which does not coincide with a translational vector of the lattice and hence generates an APB. This is illustrated in the schematic displayed in Fig. 6, where the $MgAl_2O_4$ and Fe_3O_4 lattices are shown in (100) projection at the bottom and top, respectively. The large misfit of 3.4% is accommodated by two missing planes, an Fe plane, and an Fe-O plane, resulting in the Burgers vector of $\frac{1}{4}[010]$ in (100) projection. As a result the APB marked by the arrow is formed. However, in contrast to the schematic, the APB detected in Fig. 4 seem not to follow a well-defined lattice plane, which can be concluded from the absence of a well-defined "faulty" arrangement of atomic columns. Interestingly, the initial density of APBs has to be related to the density of partial dislocations within the interface. The fact that the misfit dislocations have partial Burgers vectors can be explained by the long Burgers vector of a perfect dislocation of 0.58 nm, which forces a perfect dislocation to dissociate into partial dislocations for energetic reasons.

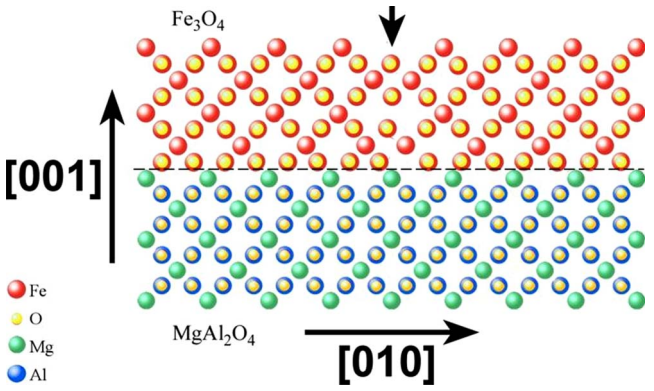

FIG. 6. (Color online) Schematic of the APB observed by high-resolution TEM (Fig. 4). The formation of the misfit dislocation with a Burgers vector component of $\frac{1}{4}[010]$ in the (100) plane, results in an APB within the Fe_3O_4 film, which is indicated by the arrow. (Fe: red, O: yellow, Mg: green, Al: blue).

V. CONCLUSIONS

From the strain relaxation studies of epitaxial Fe_3O_4 thin films grown on $MgAl_2O_4$ substrates we infer that the films show a strain-relaxation behavior consistent with the FKR model ($t_c \sim 5$ nm) predictions. Even though APBs are not expected in Fe_3O_4 films grown on $MgAl_2O_4$, TEM studies clearly revealed the formation of APBs. The presence of APBs is explained by the formation of misfit dislocations with partial Burgers vectors. These conclusions could be applicable to other spinel and nonspinel systems which are known to have APBs.

ACKNOWLEDGMENTS

This work was supported by the Science Foundation of Ireland (SFI) under Contract No. 00/PI.1/C042.

*Corresponding author; sofins@tcd.ie

[1] I. Zutic, J. Fabian, and S. Das Sharma, Rev. Mod. Phys. **76**, 323 (2004).
[2] M. Ziese, Rep. Prog. Phys. **65**, 143 (2002).
[3] J. M. D. Coey and M. Venkatesan, J. Appl. Phys. **91**, 8345 (2002).
[4] A. Yanase and N. Hamada, J. Phys. Soc. Jpn. **68**, 1607 (1999).
[5] Y. S. Dedkov, U. Rüdiger, and G. Güntherodt, Phys. Rev. B **65**, 064417 (2002).
[6] S. Lee, A. Fursina, J. T. Mayo, C. T. Yavuz, V. L. Colvin, R. G. S. Sofin, I. V. Shvets, and D. Natelson, Nature Mater. **7**, 130 (2008).
[7] A. V. Ramos, J. B. Moussy, M. J. Guittet, M. Gautier-Soyer, C. Gatel, P. Bayle-Guillemaud, B. Warot-Fonrose, and E. Snoeck, Phys. Rev. B **75**, 224421 (2007).
[8] M. Ziese, A. Bollero, I. Panagiotopoulos, and N. Moutis, Appl. Phys. Lett. **88**, 212502 (2006).
[9] A. Odagawa, Y. Katoh, Y. Kanzawa, Z. Wei, T. Mikawa, S. Muraoka, and T. Takagi, Appl. Phys. Lett. **91**, 133503 (2007).
[10] H. Qiu, L. Pan, and L. Li, J. Appl. Phys. **102**, 113913 (2007).
[11] S. K. Arora, R. G. S. Sofin, and I. V. Shvets, Phys. Rev. B **72**, 134404 (2005).
[12] S. K. Arora, Han-Chun Wu, R. J. Choudhary, I. V. Shvets, O. N. Mryasov, Hongzhi Yao, and W. Y. Ching, Phys. Rev. B **77**,

134443 (2008).
[13] H. Li, Y. Wu, Z. Guo, S. Wang, K. L. Teo, and T. Veres, Appl. Phys. Lett. **86**, 252507 (2005).
[14] J. D. Wei, I. Knittel, U. Hartmann, Y. Zhou, S. Murphy, I. V. Shvets, and F. T. Parker, Appl. Phys. Lett. **89**, 122517 (2006).
[15] T. Kasama, R. E. Dunin-Borkowski, and W. Eerenstein, Phys. Rev. B **73**, 104432 (2006).
[16] L. McGuigan, R. C. Barklie, R. G. S. Sofin, S. K. Arora, and I. V. Shvets, Phys. Rev. B **77**, 174424 (2008).
[17] W. Eerenstein, T. T. M. Palstra, T. Hibma, and S. Celotto, Phys. Rev. B **66**, 201101 (2002).
[18] J. P. Hong, S. B. Lee, Y. W. Jung, J. H. Lee, K. S. Yoon, K. W. Kim, C. O. Kim, and C. H. Lee, Appl. Phys. Lett. **83**, 1590 (2003).
[19] M. Ziese, Phys. Rev. B **62**, 1044 (2000).
[20] D. T. Margulies, F. T. Parker, F. E. Spada, R. S. Goldman, J. Li, R. Sinclair, and A. E. Berkowitz, Phys. Rev. B **53**, 9175 (1996).
[21] T. Hibma, F. C. Voogt, L. Niesen, P. A. A. van der Heijden, W. J. M. de Jonge, J. J. T. M. Donkers, and P. J. van der Zaag, J. Appl. Phys. **85**, 5291 (1999).
[22] S. M. Watts, K. Nakajima, S. van Dijken, and J. M. D. Coey, J. Appl. Phys. **95**, 7465 (2004).
[23] S. Kale, S. M. Bhagat, S. E. Loafland, T. Scabarozi, S. B. Ogale, A. Orozco, S. R. Shinde, T. Venkatesan, B. Hannoyer, B. Mercey, and W. Prellier, Phys. Rev. B **64**, 205413 (2001).
[24] M. Ziese, R. Hohne, H. C. Semmelhack, H. Reckentin, N. H. Hong, and P. Esquinazi, Eur. Phys. J. B **28**, 415 (2002).
[25] D. Reisinger, M. Schonecke, T. Brenninger, M. Opel, A. Erb, L. Alff, and R. Gross, J. Appl. Phys. **94**, 1857 (2003).
[26] W. Eerenstein, T. T. M. Palstra, S. S. Saxena, and T. Hibma, Phys. Rev. Lett. **88**, 247204 (2002).
[27] M. Ziese and J. Blythe, J. Phys.: Condens. Matter **12**, 13 (2000).
[28] S. K. Arora, R. G. S. Sofin, I. V. Shvets, and M. Luysberg, J. Appl. Phys. **100**, 073908 (2006).
[29] J. B. Moussy, S. Gota, A. Bataille, M. J. Guittet, M. Gautier-Soyer, F. Delille, B. Dieny, F. Ott, D. Doan, P. Warin, P. Bayle-Guillemaud, C. Gatel, and E. Snoeck, Phys. Rev. B **70**, 174448 (2004).
[30] W. Eerenstein, Ph.D. thesis, University of Gröningen, 2003.
[31] A. M. Bataille, L. Ponson, S. Gota, L. Barbier, D. Bonamy, M. Gautier-Soyer, C. Gatel, and E. Snoeck, Phys. Rev. B **74**, 155438 (2006).
[32] C. A. Kleint, M. K. Krause, R. Höhne, M. Lorenz, H. C. Semmelhack, A. Schneider, D. Hesse, H. Sieber, J. Taubert, and W. Andrä, J. Phys. IV **7**, C1-593 (1997).
[33] A. Georgakilas, J. Stoemenos, K. Tsagaraki, Ph. Komninou, N. Flevaris, P. Panayotatos, and A. Christou, J. Mater. Res. **8**, 1908 (1993).
[34] A. V. Ramos, S. Matzen, J. B. Moussy, F. Ott, and M. Viret, Phys. Rev. B **79**, 014401 (2009).
[35] M. Lentzen, Ultramicroscopy **99**, 211 (2004).
[36] W. Kündig and R. S. Hargrove, Solid State Commun. **7**, 223 (1969).
[37] R. Aragón, D. J. Buttrey, J. P. Sheperd, and J. M. Honig, Phys. Rev. B **31**, 430 (1985).
[38] A. Fischer, H. Kuhne, and H. Richter, Phys. Rev. Lett. **73**, 2712 (1994).